Bull. Mater. Sci., Vol. 34, No. 3, June 2011, pp. 469–475. © Indian Academy of Sciences.

Synthesis, growth, optical, mechanical and electrical properties of *L*-lysine *L*-lysinium dichloride nitrate (*L*-LLDN) single crystal

V VASUDEVAN, R RAMESH BABU*, A REICHER NELCY, G BHAGAVANNARAYANA† and K RAMAMURTHI

Crystal Growth and Thin Film Laboratory, Department of Physics, Bharathidasan University, Tiruchirappalli 620 024, India
†Materials Characterization Division, National Physical Laboratory, New Delhi 110 012, India

MS received 25 September 2010

Abstract. Semi-organic nonlinear optical material, *L*-lysine *L*-lysinium dichloride nitrate ($2C_6H_{15}N_2O_2^+ \cdot H^+ \cdot NO_3^- \cdot 2Cl^-$) was synthesized at room temperature. Single crystals of *L*-LLDN were grown by slow cooling solution growth technique. The grown crystal was confirmed by powder X-ray diffraction analysis. The crystalline perfection of the grown single crystal was characterized by high-resolution X-ray diffraction (HRXRD) studies. The cut-off wavelength was determined by UV-vis transmission spectral analysis. The frequency doubling of the grown crystal was confirmed by powder second harmonic generation (SHG) measurement. The refractive index and birefringence of the crystal were determined using He–Ne laser source. Mechanical property of the crystal was determined by Vickers hardness tester. The frequency and temperature dependence of dielectric constant (ε_r), dielectric loss (tan δ) and a.c. conductivity (σ_{ac}) were also measured.

Keywords. Nonlinear optical material; crystal growth; high-resolution X-ray diffraction; refractive index; birefringence; dielectric materials.

1. Introduction

In recent years, great efforts have been made to develop new organic, inorganic and semi-organic nonlinear optical (NLO) crystals due to their widespread applications such as frequency conversion, high-speed information processing, optical communications, and optical data storage (Sasaki and Yokotani 1990; Tsunesada *et al* 2002; Zhang *et al* 2008). In the field of nonlinear optical crystal growth, amino acids play a vital role. Amino acids exhibit natural chiral properties and crystallize in the non-centrosymmetric space groups, which is an essential criterion for NLO applications. In addition, amino acids possess particular features, such as weak Van der Waals and hydrogen bonds, wide transparency range in the visible region and zwitterionic nature of the molecules. Complexes of amino acids with inorganic salts are promising materials for optical second harmonic generation (SHG) as they tend to combine the advantages of organic amino acid and inorganic salt. Crystalline salts of optically active amino acids such as *L*-arginine, *L*-histidine, *L*-lysine, etc have been intensively studied for NLO applications. Extensive investigations in this direction resulted in the discovery of a series of *L*-lysine based amino acid compounds. The vibrational spectra and SHG studies of *L*-lysine with *L*-tartaric, *D*,*L*-malic, acetic, arsenous, and fumaric acids were reported (Marchewka *et al* 2003). *L*-lysine lysinium dichloride nitrate is one of the amino acid based semi-organic materials and the crystal structure was reported (Srinivasan *et al* 2001). It belongs to orthorhombic crystallographic system and space group $P2_12_12_1$, with cell parameters $a = 4{\cdot}984$ Å, $b = 20{\cdot}604$ Å, $c = 20{\cdot}663$ Å, $V = 2122{\cdot}1$ Å^3 and $Z = 4$. The vibrational spectral analysis of *L*-lysine *L*-lysinium dichloride nitrate was reported in literature (Briget Mary *et al* 2005). But, no reports are available on bulk crystal growth and systematic studies of *L*-lysine lysinium dichloride nitrate (abbreviated as *L*-LLDN hereafter). Thus, we have tried to grow reasonable size of *L*-LLDN crystals for NLO applications. In the present work, *L*-lysine *L*-lysinium dichloride nitrate (*L*-LLDN) was synthesized and the crystals were grown by slow cooling solution growth technique. The grown crystals were characterized by powder X-ray diffraction, HRXRD studies, UV-vis spectral analysis, SHG test, refractive index and birefringence measurements, microhardness and dielectric studies.

2. Experimental

2.1 *Synthesis and crystal growth*

L-lysine monohydrochloride and nitric acid (AR grade) in 2:1 stoichiometric ratio were taken to synthesize *L*-LLDN

*Author for correspondence (rameshbabu@physics.bdu.ac.in)

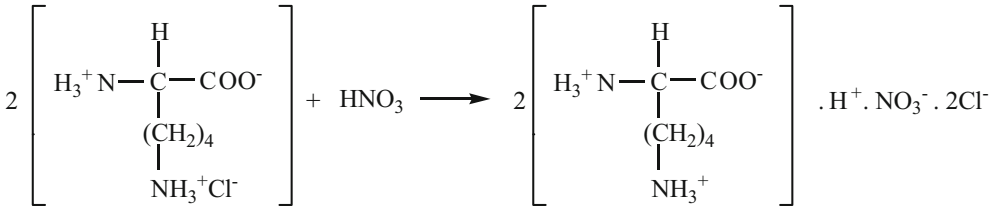

Scheme 1. Synthesis mechanism of *L*-LLDN.

according to the chemical reaction given in scheme 1. To avoid decomposition low temperature was maintained during preparation of the solution in deionized water.

The calculated amount of starting materials was dissolved in deionized water and the solution was stirred to ensure homogeneous temperature and concentration over the entire volume of the solution. The prepared solution was allowed to dry at room temperature and the salts were obtained. The purity of the synthesized salt was further increased by successive recrystallization process. *L*-LLDN exhibits a high solubility in water compared to organic solvents. The solubility of *L*-LLDN at different temperatures was measured and analysed gravimetrically. The result indicates that it has relatively high solubility and large positive solubility temperature coefficient. Thus, single crystals could be grown both by slow cooling and slow evaporation in aqueous solution. In the present work, single crystals of *L*-LLDN were grown from its saturated aqueous solution by slow cooling solution growth technique. The solution was saturated at 40°C in crystallizing container and placed inside a constant temperature bath with an accuracy of ±0·01°C. The temperature of the bath was reduced at a controlled rate of 0·2°C per day and nucleation was obtained at 38°C. Well defined hexagonal morphology transparent single crystals of *L*-LLDN with dimensions 16 × 16 × 6 mm^3 were harvested from the mother solution after a period of one week and the grown crystals are shown in figure 1.

2.2 *Characterization*

The cell parameters of the grown crystal were determined from the powder X-ray diffraction pattern using standard software. The optical transmission spectrum was recorded in the range 200–1100 nm using Lambda 35 UV-vis-NIR spectrometer for a crystal of thickness 1 mm. The powder SHG measurement was carried out using Q-Switched high energy Nd:YAG laser (1064 nm – SPITLIGHT 600-10 model) with a pulse width of 6 ns. Refractive index and birefringence measurements were carried out using He–Ne laser source in the wavelength of 632·8 nm. The microhardness of the crystal was measured using a microhardness tester (HMV-2) fitted with a Vickers diamond pyramidal indenter and attached with an optical microscope. Dielectric measurements were carried out using HIOKI 3532–50 LCR meter in the frequency range 100 kHz–2 MHz. To provide electrical contact, the cut and polished rectangular shaped single crystals were coated with high grade silver paste on parallel faces. The coated samples were placed between the two copper electrodes forming parallel plate capacitor with dielectric sample. The dielectric behaviour of the *L*-LLDN single crystal was measured after applying suitable voltage across the sample.

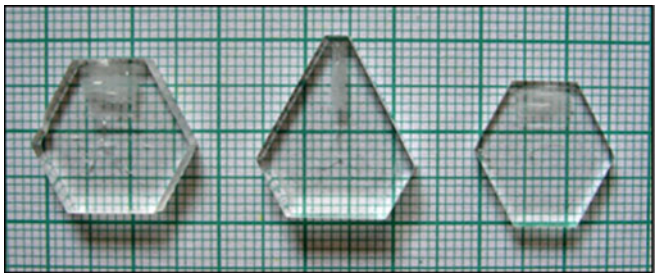

Figure 1. Grown single crystals of *L*-LLDN.

The crystalline perfection of the grown single crystals was characterized by HRXRD by employing a multicrystal X-ray diffractometer developed at NPL (Lal and Bhagavannarayana 1989). The well-collimated and monochromated MoKα_1 beam obtained from the three monochromator Si crystals set in dispersive (+,−,−) configuration has been used as exploring X-ray beam. The specimen crystal is aligned in the (+,−,−,+) configuration. Due to dispersive configuration, though the lattice constant of the monochromator crystal(s) and the specimen are different, the unwanted dispersion broadening in the diffraction curve (DC) of the specimen crystal is insignificant. The specimen can be rotated about the vertical axis, which is perpendicular to the plane of diffraction, with minimum angular interval of 0·4 arc s. The rocking or diffraction curves were recorded by changing the glancing angle (angle between the incident X-ray beam and the surface of the specimen) around the Bragg diffraction peak position, θ_B (taken as zero for the sake of convenience) starting from a suitable arbitrary glancing angle and ending at a glancing angle after the peak so that all the meaningful scattered intensities on both sides of the peak are included in the diffraction curve. The DC was recorded by the so-called ω scan wherein the detector was kept at the same angular position, $2\theta_B$, with wide opening for its slit. This arrangement is very appropriate to record the short range order scattering caused by the defects or by the scattering from local Bragg diffractions from agglomerated point defects or due to

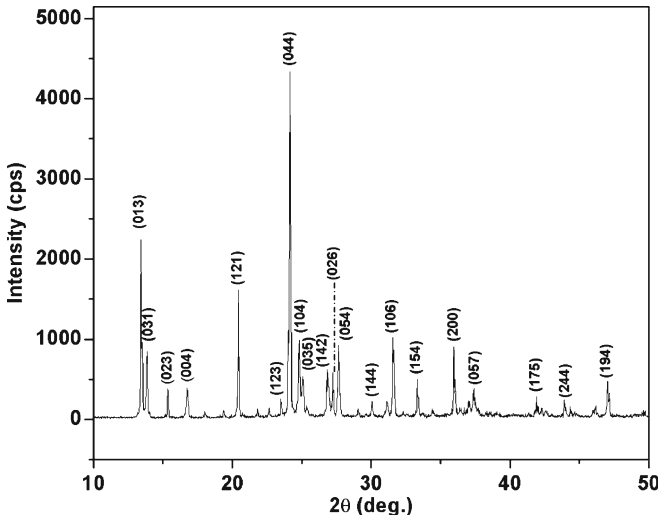

Figure 2. Powder XRD pattern of *L*-LLDN crystal.

low angle and very low angle structural grain boundaries (Bhagavannarayana and Kushwaha 2010). Before recording the diffraction curve to remove the non-crystallized solute atoms remaining on the surface of the crystal and the possible layers which may sometimes form on the surfaces of crystals grown by solution methods (Bhagavannarayana *et al* 2006) and also to ensure surface planarity, the specimen was first lapped and chemically etched in a nonpreferential etchant of water and acetone mixture in 1:2 volume ratio.

3. Results and discussion

3.1 *Powder XRD analysis*

Figure 2 shows the powder XRD pattern of *L*-LLDN crystal. 2θ values from various diffraction planes and the corresponding intensities are collected. The calculated lattice parameters values, $a = 4{\cdot}973$ Å, $b = 20{\cdot}471$ Å, $c = 20{\cdot}780$ Å and $V = 2115{\cdot}60$ Å^3, are consistent with the results reported using the single crystal X-ray diffraction (Srinivasan *et al* 2001). The calculated lattice parameters are compared with reported values and are given in table 1. The well-defined sharp diffraction peaks reveal that the grown crystals are of good crystalline quality.

Table 1. Lattice parameters of *L*-LLDN single crystal.

Lattice parameters	Calculated values	Reported values
a (Å)	4·973	4·984
b (Å)	20·471	20·604
c (Å)	20·780	20·663
V (Å^3)	2115·60	2122·1

3.2 *High-resolution X-ray diffraction (HRXRD) studies*

Figure 3 shows the high-resolution diffraction curve (DC) recorded for a typical solution grown *L*-LLDN single crystal using (013) diffracting planes in symmetrical Bragg geometry by employing the multicrystal X-ray diffractometer with MoKα_1 radiation. As seen in the figure, the DC contains a single peak and indicates that the specimen is free from structural grain boundaries. The full width at half maximum (FWHM) of the curve is 28 arc s which is somewhat more than that expected for an ideally perfect crystal from the plane wave theory of dynamical X-ray diffraction (Batterman and Cole 1964), but close to that expected for a nearly perfect real life crystal.

It is interesting to see the asymmetry of the DC. For a particular angular deviation ($\Delta\theta$) of glancing angle with respect to the peak position, the scattered intensity is much more in the positive direction in comparison to that of the negative direction. This feature clearly indicates that the crystal contains predominantly interstitial type of defects than that of vacancy defects. This can be well understood by the fact that due to interstitial defects (self interstitials or impurities at interstitial sites), which may be due to fast growth and/or impurities present in the raw material, the lattice around these defects undergo compressive stress (Bhagavannarayana *et al* 2008) and the interplanar distance '*d*' decreases and leads to give more scattered (also known as diffuse X-ray scattering) intensity at slightly higher Bragg angles (θ_B) as d and sin θ_B are inversely proportional to each other in the Bragg equation ($2d \sin\theta_B = n\lambda$; n and λ being the order of reflection and wavelength, respectively which are fixed). However, the single diffraction curve with reasonably low FWHM indicates that the crystalline perfection is fairly good. The density of such interstitial defects is, however, very meagre and in almost all real crystals including nature gifted crystals, such defects are commonly observed and are many times

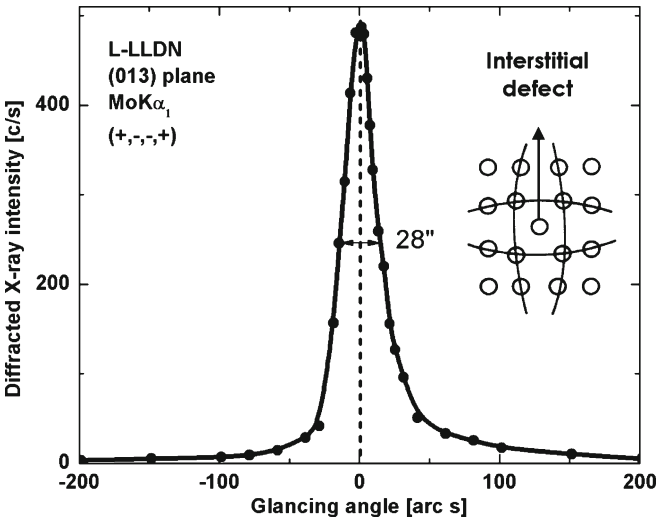

Figure 3. HRXRD curve recorded for *L*-LLDN crystal.

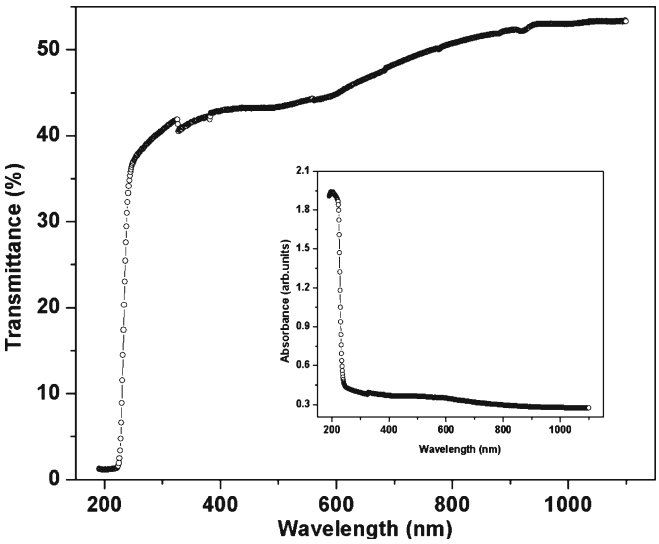

Figure 4. UV–vis–NIR spectra of *L*-LLDN single crystal.

unavoidable due to thermodynamical conditions and hardly affect the device performance. More details may be obtained from the study of high-resolution diffuse X-ray scattering measurements (Lal and Bhagavannarayana 1989), which is, however, not the main focus of the present investigation. It is worth to mention here that the observed scattering due to interstitial defects is of short order nature as the strain due to such minute defects is limited to the very defect core and the long order could not be expected and hence the change in the lattice parameter of the crystal is not possible. It may be mentioned here that the minute information like the asymmetry in the DC could be possible as in the present sample only because of the high-resolution of the multicrystal X-ray diffractometer used in the present investigation.

3.3 *UV–vis–NIR spectral analysis*

The transmission spectrum of *L*-LLDN crystal is shown in figure 4. It is observed that the grown *L*-LLDN crystal has lower cutoff wavelength at 224 nm and good transmission in the entire visible region. This is the most desirable property of the crystals used for NLO applications. *L*-lysine based crystals often possess lower transparency cutoff, which is the intrinsic properties of *L*-lysine (Sun *et al* 2009). The absorption spectrum of *L*-LLDN crystal is shown in the inset of figure 4.

3.4 *Second harmonic generation (SHG) test*

The grown *L*-LLDN single crystal was ground into powder and closely packed between two transparent glass slides. The powdered samples were irradiated by an incident radiation of pulse width 6 ns from a Q-switched high energy Nd:YAG laser (1064 nm). Green light emission (532 nm) was observed at the output which is exactly half of the input wavelength. This confirms that the frequency of the input was doubled at the output. Therefore, *L*-LLDN single crystal generates second harmonic frequency. The SHG efficiency of the *L*-LLDN crystal is about 1·06 times that of the standard KDP crystal.

3.5 *Refractive index measurement*

The refractive index of the *L*-LLDN crystal was determined by Brewster's angle method. A polished single crystal of *L*-LLDN with 1 mm thickness was mounted on a rotating mount at an angle varying from 0 to 90 degrees. The angular reading on the rotary stage was observed, when the crystal was perfectly perpendicular to the intra-cavity beam. The crystal was rotated until the reflection of laser light vanishes and this angle has been noted. Brewster's angle (θ_p) for *L*-LLDN was measured to be 54·5°. The refractive index was calculated using the formula $n = \tan\theta_p$, and found to be 1·40.

3.6 *Birefringence measurements*

Refractive index and birefringence are the most important material parameters for calculating phase matching angles (Fischer and Ohmer 1995) and to study the perfection of crystals. The cut and polished *L*-LLDN single crystal of 1 mm thickness was used for this measurement. He–Ne laser source passed through the crystal (along the optical plane) placed between crossed polarizer and analyser, the transmitted light from the analyser undergoes interference and fringe pattern was observed on the screen as shown in figure 5. The sample was rotated to capture interference pattern from different points of specimen to assess the optical quality of the grown crystal. The fringes are distorted as shown in figure 5(a–c), it may be due to various type of defects present in the crystal-like scattering centres, strains in the crystal during the growth, inclusion of solvents, interstitial type of defects, etc. HRXRD studies evidently show the presence of interstitial type of defects. The intensity of the light emergence from the crystal also decreases due to these defects as shown in figure 5c.

A power meter was used to detect the light transmitted through the analyser. Initially the polarizer and analyser were adjusted to be in crossed position. The birefringence (Δn) can be calculated using the following relation (Nasr 2007)

$$\Delta n = \frac{\lambda}{\pi t} \sin^{-1} \sqrt{\frac{I}{I_0}},$$

where I_0 is the intensity of light before passing through the sample, I the intensity of light reaching the detector and t the thickness of the sample. When the angle of incidence of the polarized beam incident on the sample is varied, maximum intensity was noted. The birefringence value of *L*-LLDN

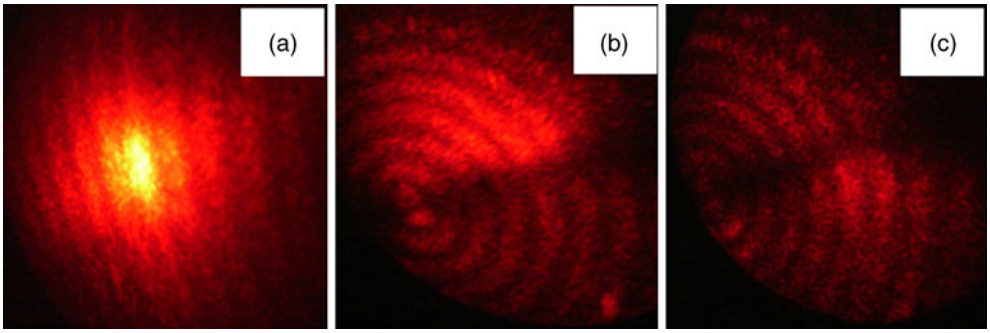

Figure 5. Interference fringe patterns of *L*-LLDN single crystal.

crystal was determined to be 0·00247. Using this technique, the exact direction of optic axis of the grown crystal could also be determined. This further extends the use of birefringence in obtaining seeds for directional growth along the optic axis. Comparisons of birefringence value of some other crystals (Kar *et al* 2008, 2009) are given in table 2.

3.7 *Microhardness test*

Hardness of the material is defined as the resistance it offers to the motion of dislocations, deformations or damage under an applied stress. For hardness measurement, crystal with a thickness of 3 mm was used and loads of different magnitudes were applied. Vickers hardness number (H_v) was calculated from the equation

$$H_v = 1{\cdot}8544P/l^2, \text{kg/mm}^2,$$

where P is the applied load in kg and l the average diagonal length in mm. The calculated values are 8·41, 10·55 and 12·25 kg mm^{-2} for the applied load of 25, 50 and 100 g, respectively. From the results it was observed that the hardness value increases up to 100 g and then cracks started to appear with further increase in applied load.

3.8 *Dielectric properties*

The frequency and temperature response of dielectric properties of *L*-LLDN crystal were studied. The values of capacitance (C_p) and loss (tan δ) were obtained from the dielectric measurement. Other parameters such as dielectric constant, ε_r and conductivity, σ_{ac}, are calculated using the formula

$$\varepsilon_r = C_p t/\varepsilon_o A; \quad \sigma_{ac} = 2\pi f \varepsilon_o \varepsilon_r \tan\delta,$$

where t is the thickness of the sample, ε_o the permittivity of free space ($\varepsilon_o \approx 8{\cdot}854 \times 10^{-12}$ F/m), A the area of the sample, f the frequency of applied field.

Figures 6(a–c) show the frequency dependency of dielectric constant, dielectric loss and a.c. conductivity of *L*-LLDN crystal. From the frequency response of the dielectric constant (ε_r), it was found that the dielectric constant increases initially at low frequencies and decreases further increasing the frequency as shown in figure 6a. This can be understood that the frequency of the electric field is equal to that of natural frequency of bound charge which tends to oscillate the molecules with high energy and hence the dielectric constant increases initially at low frequencies. At higher frequencies, the dielectric constant decreases due to the frequency of the electric field which is not equal to that of natural frequency of the bounded charge. Moreover, at low frequencies all mechanisms such as space charge, orientation, ionic and electronic polarizations are operative hence the dielectric constant is maximum. At higher frequencies, these mechanisms cannot follow the applied electric field; therefore, the dielectric constant is low. The dielectric loss also exhibits similar behaviour with increasing frequency as shown in figure 6b. Increase of dielectric loss at low frequencies is attributed to oscillation of dipoles. At higher frequencies all the polarization mechanisms are not operative, hence energy need not to be spent to rotate dipoles, therefore, dielectric loss is also minimum. Figure 6c shows the frequency response of a.c. electrical conductivity and it increases with increasing frequency.

Figures 7(a–c) show the temperature variation of the dielectric constant, dielectric loss and a.c. conductivity of *L*-LLDN crystal. It was observed that the dielectric constant decreases with increasing temperature as shown in figure 7a. This can be explained by the contribution of ionic, electronic, dipolar and space charge polarizations in the crystal with respect to temperature. The ionic and electronic polarizations decrease with an increase in temperature. This is because, increasing temperature increases the atomic distances which affect

Table 2. Comparison of birefringence value of some other crystals measured using He–Ne laser source.

Crystal	Birefringence (Δn)	References
Fe:$LiNbO_3$	0·001898*	(Kar *et al* 2008)
	0·074**	
Mn:$Li_2B_4O_7$	0·003894	(Kar *et al* 2009)
L-LLDN	0·00247 ± 0·001	Present work

* Perpendicular to the sample; ** perpendicular to the optic axis.

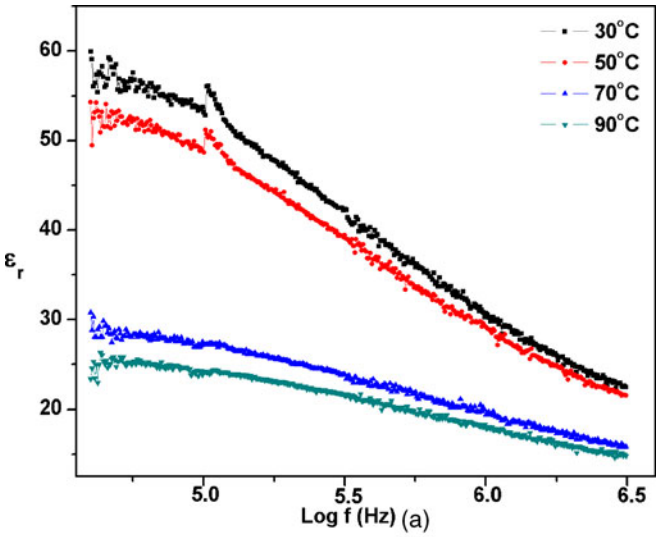

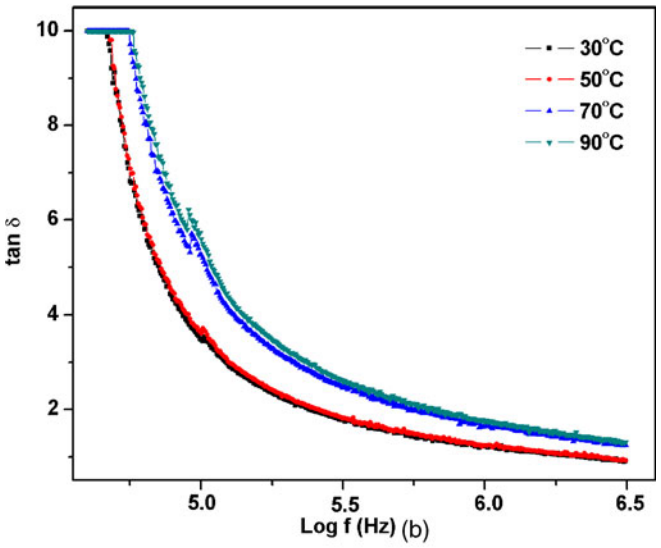

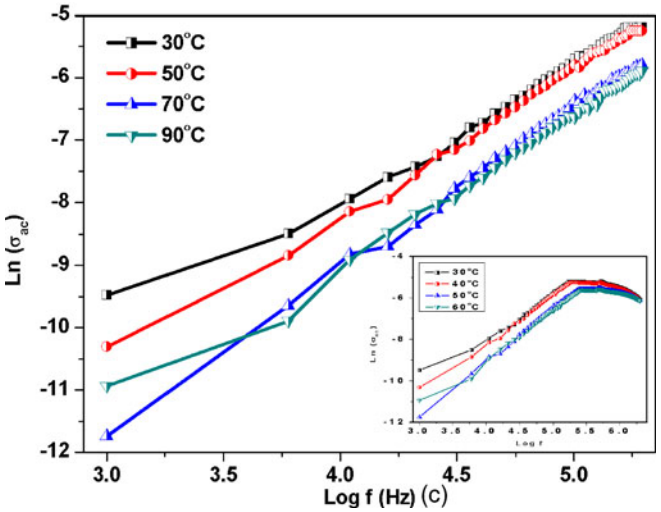

Figure 6(a–c). Frequency dependence of ε_r, tan δ and σ_{ac} for *L*-LLDN crystal.

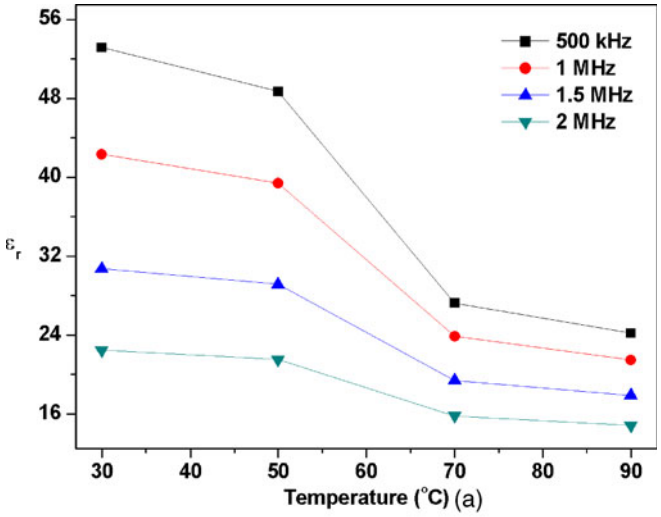

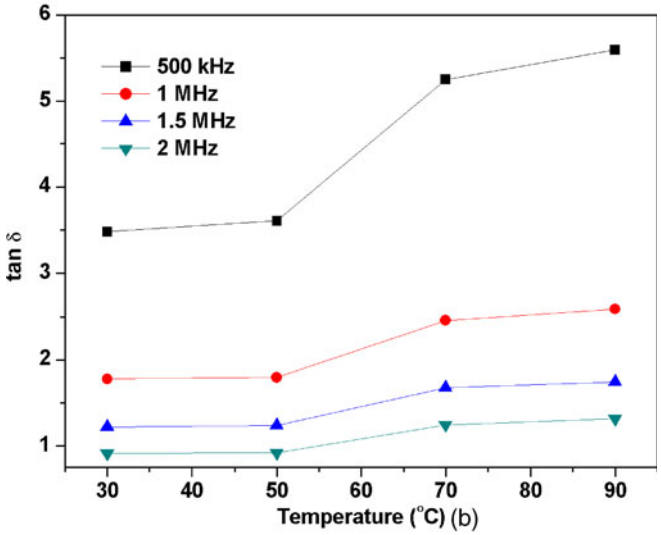

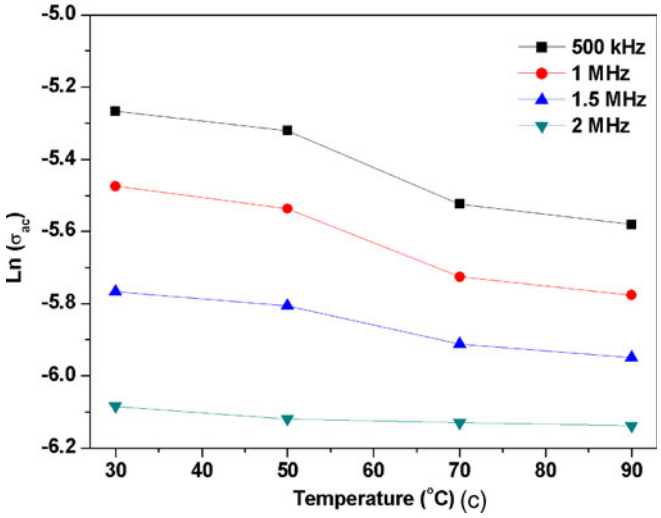

Figure 7(a–c). Temperature dependence of ε_r, tan δ and σ_{ac} for *L*-LLDN crystal.

both the ionic as well as the electronic contributions to polarization (Agrawal and Rao 1970). The dipolar polarization, being inversely proportional to the temperature, obviously decreases with temperature. The contribution to the polarization from the space charge will depend on the purity and perfection of the crystals. Furthermore, when increasing the temperature the volume of the crystal expands and the contribution of polarizable molecules decrease in number per unit volume thus the dielectric constant decreases (Bosman and Havinga 1963). The dielectric loss also decreases with increasing temperature as shown in figure 7b. The temperature variation of a.c. electrical conductivity decreases with increasing temperature due to thermal expansion of the crystal shown in figure 7c. When increasing the temperature the density of the crystal is reduced by thermal expansion (Sindhu *et al* 2002) and thus decreases the conductivity.

4. Conclusions

L-LLDN single crystals were successfully grown by slow cooling solution growth technique. The cell parameters were collected from the powder X-ray diffraction analysis, and are well in agreement with the reported values. HRXRD studies indicate that the crystal contains interstitial defect and the full width at half maximum was found to be 28 arc s which reveals that quality of the grown crystal is good. The crystal is transparent in the UV-visible region and the cutoff wavelength is 224 nm. From the powder SHG measurement, it can be concluded that *L*-LLDN single crystals generate second harmonic frequency which is 1·06 times better than that of standard KDP. Refractive index and birefringence of the grown crystal were measured to be 1·40 and 0·00247, respectively. Hardness of the crystal was found to be increasing up to a load of 100 g and cracks were started with further increase in load. From dielectric measurement, it was observed that the two effects contributing to the temperature dependence of dielectric constant decrease the number of polarizable molecules per unit volume which is a direct result of the volume expansion and the contribution of various polarization mechanisms.

Acknowledgements

The authors (VV) and (RR) would like to gratefully acknowledge the Council of Scientific and Industrial Research (CSIR), Government of India, for financial support (Grant No. 03/(1105)/08/EMR/II). Also one of the authors (VV) is grateful to the Council of Scientific and Industrial Research, Government of India, for providing a senior research fellowship.

References

Agrawal M D and Rao K V 1970 *J. Phys. C: Solid State Phys.* **3** 1120

Batterman B W and Cole H 1964 *Rev. Mod. Phys.* **36** 681

Bhagavannarayana G and Kushwaha S K 2010 *J. Appl. Crystallogr.* **43** 154

Bhagavannarayana G, Parthiban S and Meenakshisundaram S 2006 *J. Appl. Crystallogr.* **39** 784

Bhagavannarayana G, Parthiban S and Meenakshisundaram S 2008 *Cryst. Growth Des.* **8** 446

Bosman A J and Havinga E E 1963 *Phys. Rev.* **129** 1593

Briget Mary M, Umadevi M and Ramakrishnan V 2005 *Spectrochim. Acta A* **61** 3124

Fischer D W and Ohmer M C 1995 *J. Appl. Phys.* **77** 5942

Kar S, Verma S, and Bartwal K S 2008 *Cryst. Growth Des.* **8** 4424

Kar S, Verma S and Bartwal K S 2009 *Cryst. Res. Technol.* **44** 305

Lal K and Bhagavannarayana G 1989 *J. Appl. Crystallogr.* **22** 209

Marchewka M K, Debrus S and Ratajczak H 2003 *Cryst. Growth Des.* **3** 587

Nasr A M 2007 *Int. J. Mater. Sci.* **2** 103

Sasaki T and Yokotani A 1990 *J. Cryst. Growth* **99** 820

Sindhu S, Anantharaman M R, Thampi B P, Malini K A and Kurian P 2002 *Bull. Mater. Sci.* **25** 599

Srinivasan N, Sridhar B and Rajaram R K 2001 *Acta Crystallogr.* **E57** 888

Sun Z H, Xu D, Wang X Q, Zhang G H, Yu G, Zhu L Y and Fan H L 2009 *Mater. Res. Bull.* **44** 925

Tsunesada F, Iwai T, Watanabe T, Adachi H, Yoshimura M, Mori Y and Sasaki T 2002 *J. Cryst. Growth* **237–239** 2104

Zhang Y, Li H, Xi B, Che Y and Zheng J 2008 *Mater. Chem. Phys.* **108** 192